SSII cancellation in an EAM-based OFDM-IMDD transmission system employing a novel dynamic chirp model

Dar-Zu Hsu,[1,3] Chia-Chien Wei,[2,*] Hsing-Yu Chen,[1,3] Yi-Cheng Lu,[1] Cih-Yuan Song,[1] Chih-Chieh Yang,[1] and Jyehong Chen[1]

[1]*Department of Photonics, National Chiao-Tung University, Hsinchu, 300, Taiwan*
[2]*Department of Photonics, National Sun Yat-sen University, Kaohsiung, 804, Taiwan*
[3]*Information and Communications Research Labs, Industrial Technology Research Institute, Hsinchu, 310, Taiwan*
ccwei@mail.nsysu.edu.tw

Abstract: We develop a novel subcarrier-to-subcarrier intermixing interference (SSII) cancellation technique to estimate and eliminate SSII. For the first time, the SSII cancellation technique is experimentally demonstrated in an electro-absorption modulator- (EAM-) based intensity-modulation-direct-detection (IMDD) multi-band OFDM transmission system. Since the characteristics of SSII are seriously affected by the chirp parameter, a simple constant chirp model, we found, cannot effectively remove the SSII. Therefore, assuming that the chirp parameter linearly depends on the optical power, a novel dynamic chirp model is developed to obtain better estimation and cancellation of SSII. Compared with 23.6% SSII cancellation by the constant chirp model, our experimental results show that incorporating the dynamic chirp model into the SSII cancellation technique can achieve up to 74.4% SSII cancellation and 2.8-dB sensitivity improvement in a 32.25-Gbps OFDM system over 100-km uncompensated standard single-mode fiber.

OCIS codes: (060.2330) Fiber optics communications; (060.0060) Fiber optics and optical communications.

References and links

1. T. Koonen, "Fiber to the home/fiber to the premises: what, where, and when?" Proc. IEEE **94**(5), 911–934 (2006).
2. G. Talli, C. W. Chow, E. M. MacHale, C. Antony, R. Davey, P. D. Townsend, T. De Ridder, X. Z. Qiu, P. Ossieur, H. G. Krimmel, D. W. Smith, I. Lealman, A. Poustie, S. Randel, and H. Rohde, "Long reach passive optical networks," in *The 20th Annual Meeting of the IEEE Lasers and Electro-Optics Society, 2007. LEOS 2007*, (IEEE-LEOS, 2007), pp. 868–869.
3. R. Lin, "Next generation PON in emerging networks," in *Optical Fiber Communication Conference and Exposition and The National Fiber Optic Engineers Conference*, OSA Technical Digest (CD) (Optical Society of America (2008), paper OWH1.
4. R. P. Davey, D. B. Grossman, M. Rasztovits-Wiech, D. B. Payne, D. Nesset, A. E. Kelly, A. Rafel, S. Appathurai, and S. H. Yang, "Long-reach passive optical networks," J. Lightwave Technol. **27**(3), 273–291 (2009).
5. K. Y. Cho, K. Tanaka, T. Sano, S. P. Jung, J. H. Chang, Y. Takushima, A. Agata, Y. Horiuchi, M. Suzuki, and Y. C. Chung, "Long-reach coherent WDM PON employing self-polarization-stabilization technique," J. Lightwave Technol. **29**(4), 456–462 (2011).
6. D. Shea and J. Mitchell, "A 10 Gb/s 1024-way-split 100-km long-reach optical-access network," J. Lightwave Technol. **25**(3), 685–693 (2007).
7. D. Z. Hsu, C. C. Wei, H. Y. Chen, W. Y. Li, and J. Chen, "Cost-effective 33-Gbps intensity modulation direct detection multi-band OFDM LR-PON system employing a 10-GHz-based transceiver," Opt. Express **19**(18), 17546–17556 (2011).
8. D. Z. Hsu, C. C. Wei, H. Y. Chen, Y. C. Lu, and J. Chen, "A 40-Gbps OFDM LR-PON system over 100-km fiber employing an economical 10-GHz-based transceiver," in *Optical Fiber Communication Conference*, OSA Technical Digest (Optical Society of America, 2012), paper OW4B.

#178232 - $15.00 USD Received 1 Nov 2012; revised 14 Dec 2012; accepted 21 Dec 2012; published 7 Jan 2013

9. A. Gharba, P. Chanclou, M. Ouzzif, J. L. Masson, L. A. Neto, R. Xia, N. Genay, B. Charbonnier, M. Hélard, E. Grard, and V. Rodrigues, "Optical transmission performance for DML considering laser chirp and fiber dispersion using AMOOFDM," in *2010 International Congress on Ultra Modern Telecommunications and Control Systems and Workshops (ICUMT)* (2010), pp. 1022–1026.
10. C. C. Wei, "Small-signal analysis of OOFDM signal transmission with directly modulated laser and direct detection," Opt. Lett. **36**(2), 151–153 (2011).
11. W. R. Peng, B. Zhang, K. M. Feng, X. Wu, A. E. Willner, and S. Chi, "Spectrally efficient direct-detected OFDM transmission incorporating a tunable frequency gap and an iterative detection techniques," J. Lightwave Technol. **27**(24), 5723–5735 (2009).
12. C. C. Wei, "Analysis and iterative equalization of transient and adiabatic chirp effects in DML-based OFDM transmission systems," Opt. Express **20**(23), 25774–25789 (2012).
13. D. Z. Hsu, C. C. Wei, H. Y. Chen, J. Chen, M. C. Yuang, S. H. Lin, and W. Y. Li, "21 Gb/s after 100 km OFDM long-reach PON transmission using a cost-effective electro-absorption modulator," Opt. Express **18**(26), 27758–27763 (2010).
14. E. O. Brigham, *Fast Fourier Transform and Its Applications*, 1st ed. (Wiley, New York, 1997).
15. F. Devaux, Y. Sorel, and J. F. Kerdiles, "Simple measurement of fiber dispersion of chirp parameter of intensity modulated light emitter," J. Lightwave Technol. **11**(12), 1937–1940 (1993).

1. Introduction

With the exponentially increasing of customer needs for broadband services, optical access networks have been considered as future-proof infrastructures, and a passive optical network (PON) is one of the most promising candidates to economically provide high bandwidth to end-users [1]. Recently, optically amplified large-split long-reach PON (LR-PON) is proposed to economically provide higher bandwidth and larger fiber coverage range [1–6], thus the capital and operational expenditures can be reduced considerably by consolidating the O/E/O conversion interfaces inside the existing networks. To reach the target of higher data rate over up to 100-km transmission distance without significant cost increase, optical intensity modulation and direct-detection (IMDD) scheme is still preferred, especially using cost-effective transmitters, such as directly modulated DFB lasers (DMLs) and electro-absorption modulated lasers (EMLs).

Combined with quadrature amplitude modulation (QAM) format, orthogonal frequency-division multiplexing (OFDM) has been envisioned as a prominent modulation scheme to effectively lower the bandwidth requirement of components. However, optical OFDM signals employing DMLs or EMLs will be optical double-side band (DSB) and frequency-chirped, resulting in detrimental dispersion- and chirp-related power fading. Since the power fading is periodic, a dynamic multi-band optical OFDM scheme [7–9] is proposed to solve the problem. In this scheme, the OFDM subcarriers can be dynamically allocated with adaptive modulation formats to the secondary passbands to make the best of bandwidth utilization. For example, the experimental results in [7,8] show that available bandwidth of 100-km standard single-mode fiber (SSMF) transmission can be increased from 3 GHz to 6 GHz after allocating OFDM subcarriers in the secondary passbands. Thus, power fading is no longer the major bottleneck of dispersion uncompensated IMDD networks. Nevertheless, in addition to power fading, optical IMDD transmission will suffer from dispersion- and chirp-related subcarrier-to-subcarrier intermixing interference (SSII), which has been theoretically and experimentally investigated in [7, 8, 10]. The investigated results show that most of SSII is overlapped with the OFDM subcarriers located in the secondary passbands to degrade the signal-to-noise ratio (SNR) of the subcarriers. Therefore, SSII becomes the major bottleneck and will reduce the performance of economical IMDD OFDM transmission systems. By applying adaptive power and modulation allocation [7], demonstrates, via both theoretical analysis and simulation, that all the subcarriers can reach a target performance under the effect of SSII. The presence of SSII, however, will decrease the modulation levels, especially those of the secondary passbands, resulting in lower data rate and spectral efficiency.

Similar to the reconstruction and elimination of subcarrier-to-subcarrier beating interference (SSBI) in a Mach-Zehnder modulator- (MZM-) based single-side band OFDM system [11], it is possible to reconstruct and mitigate SSII in an IMDD OFDM system [12].

#178232 - $15.00 USD Received 1 Nov 2012; revised 14 Dec 2012; accepted 21 Dec 2012; published 7 Jan 2013

However, in an MZM-based amplitude modulation system, OFDM signals are directly encoded in an optical field. Accordingly, SSBI is only composed of the beating terms among subcarriers due to the square-law photo-detection, but SSII includes additional intermixing terms caused by square-root-law amplitude modulation (i.e. linear intensity modulation) and chirp-induced phase modulation. Hence, unlike the case of SSBI, the amount of total SSII is a function of dispersion and chirp. In this work, the SSII cancellation technique is experimentally demonstrated in an IMDD OFDM transmission system for the first time. Based on the proposed SSII reconstruction scheme, the theoretical SSII can be calculated and used to eliminate the received SSII. To further improve the effectiveness of SSII cancelation, this work develops a dynamic chirp model that takes the voltage-dependent chirp [13] into consideration. While only 23.6% SSII is cancelled by the constant chirp model, 74.4% SSII cancellation and 2.8-dB sensitivity improvement at the FEC limit are experimentally demonstrated by incorporating the dynamic chirp model into the SSII cancellation technique in a 32.25-Gbps OFDM system over 100-km uncompensated SSMF.

2. SSII theory

In [7], the EAM model only considers the constant chirp parameter. However, in [13], we learned that the chirp parameter is a function of modulation voltage, and therefore, a new model that takes the dynamic chirp into consideration would be required. Similar to the deviation in [10], the envelop of the output optical field at the optical transmitter can be given by $E \propto \sqrt{V}\, e^{-j\Delta\phi}$, where V is the modulation voltage, $\Delta\phi$ is the chirp-induced phase modulation, approximated as $\Delta\phi \cong \alpha \log|E|$, and α is the chirp parameter. The modulation voltage of OFDM signals is expressed as $V = V_b + \sum_{n=1}^{N} \Re\{v_n e^{jn\omega t}\}$, where V_b is the bias voltage, N is the OFDM subcarrier number, $\omega/(2\pi)$ is the subcarrier spacing, and v_n is the encoded complex information of the n^{th} subcarrier, and $\Re\{\cdot\}$ represents the real part. The whole frequency response of electrical-signal-to-optical-power conversion is set as $H_T(n)$, composed of the responses of digital-to-analog conversion (DAC), electrical filter, electrical amplifier, and optical modulator, and $H_T(0)$ denotes the frequency response of the optical carrier. Thus, the power envelop can be written as $P = H_T(0)V_b + \sum_{n=1}^{N} \Re\{H_T(n)v_n e^{jn\omega t}\}$ or $P = H_T(0)V_b \times \left[1 + \sum_{n=1}^{N} \Re\{x_n e^{jn\omega t}\}\right]$, where $x_n = \left[H_T(n)/H_T(0)\right]\left[v_n/V_b\right]$ stands for the normalized OFDM signal. Setting the AC power envelop as $X_1 = \sum_{n=1}^{N} \Re\{x_n e^{jn\omega t}\}$, we could consider the power-dependent chirp parameter as $\alpha = \sum_{m=0}^{\infty} \alpha_m X_1^{\,m}$ by Taylor series, and therefore, the normalized envelop of the optical field E can be approximated as

$$E' \cong 1 + \frac{1 - j\alpha_0}{2} X_1 - \frac{1 + \alpha_0^{\,2} + 4j\alpha_1}{8} X_2, \tag{1}$$

where $X_2 = X_1^{\,2} \equiv \sum_{n=1}^{2N} \Re\{\tilde{x}_n e^{jn\omega t}\}$ is the 2nd order term, and the third and higher order terms of x_n are neglected such that only the first two terms of α are included. Here only considering α_0 is the constant chirp model [7, 10], and the dynamic chirp model will include both α_0 and α_1 so that the chirp parameter is linearly dependent on the optical power. Considering only chromatic dispersion, the response of fiber transmission after fiber of distance L with the dispersion parameter β_2 can be simplified as $H_{CD}(n) = e^{jn^2\theta_D}$, where $\theta_D = \beta_2 L \omega^2/2$. Accordingly, the optical field becomes

#178232 - $15.00 USD Received 1 Nov 2012; revised 14 Dec 2012; accepted 21 Dec 2012; published 7 Jan 2013

$$E'(L) \cong 1 + \frac{1}{2} \times \underbrace{\sqrt{1+\alpha_0^2}\, e^{-j\theta_\alpha} \sum_{n=1}^{N} \Re\{x_n e^{jn\omega t}\} e^{jn^2\theta_D}}_{X_{t1}} - \frac{1}{8} \times \underbrace{\left(1+\alpha_0^2\right) \left|\sec\theta_A\right| e^{j\theta_A} \sum_{n=1}^{2N} \Re\{\tilde{x}_n e^{jn\omega t}\} e^{jn^2\theta_D}}_{X_{t2}}, \tag{2}$$

where $\theta_\alpha \equiv \tan^{-1}\alpha_0$, $\theta_A \equiv \tan^{-1}\left(4\alpha_1 / 1+\alpha_0^2\right)$, X_{t1} represents the transmitted OFDM signal, and X_{t2} is the transmitted 2nd order nonlinear term. After square-law photo-detection, the received signal is proportional to $|E'(L)|^2 \cong 1 + \Re\{X_{t1}\} + |X_{t1}|^2/4 - \Re\{X_{t2}\}/4$, where the third order and the fourth order terms are also omitted, and $|X_{t1}|^2$ can be represented as $(1+\alpha_0^2)\sum_{n=1}^{2N} \Re\{\tilde{x}_{d,n} e^{jn\omega t}\}$. If the combined frequency responses of the receiver, including photodiode, electrical amplifier, and analog-to-digital conversion (ADC), is denoted as $H_R(n)$, the normalized received signal is

$$\begin{aligned} R'(L) \cong\ & 1 + \sqrt{1+\alpha_0^2} \sum_{n=1}^{N} H_R(n) \Re\{x_n e^{jn\omega t}\} \cos\left(n^2\theta_D - \theta_\alpha\right) \\ & + \frac{1+\alpha_0^2}{4} \times \Bigg[\underbrace{\sum_{n=1}^{2N} H_R(n) \Re\{\tilde{x}_{d,n} e^{jn\omega t}\}}_{Beating\ \ terms} - \underbrace{\left|\sec\theta_A\right| \sum_{n=1}^{2N} H_R(n) \Re\{\tilde{x}_n e^{jn\omega t}\} \cos\left(n^2\theta_D + \theta_A\right)}_{Intermixing\ \ terms} \Bigg]. \end{aligned} \tag{3}$$

The 2nd term at the RHS of $R'(L)$ corresponds to the desired OFDM signal; the 3rd term indicates the beating terms among subcarriers due to the square-law photo-detection, and the last term represents the intermixing terms caused by square-root-law amplitude modulation and chirp-induced phase modulation. Then, the combination of the 2nd order terms is the so-called SSII, and denoted as the theoretical $SSII_T$ in this work. From the SSII theory, not only the chirp parameters of α_0 and α_1, and the responses of H_T, H_{CD} and H_R, but also the complex information of v_n are necessary to calculate the SSII. Although the transmitted data are never exactly known at the receiver, the received data after hard decision are used as v_n to estimate SSII, and an iterative process could be employed to improve the accuracy of SSII estimation.

3. SSII cancellation technique

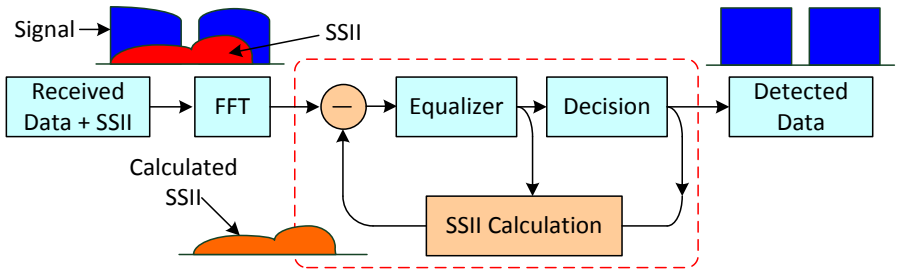

Fig. 1. The block diagram of the SSII cancellation technique.

To mitigate the influence of SSII, we introduce the SSII cancellation technique at the receiver and the block diagram is shown in Fig. 1. The received OFDM data with SSII are demodulated and detected as the normal OFDM demodulation process, including fast Fourier transform (FFT), equalization, and decision. Then the detected data are used as v_n to calculate

#178232 - $15.00 USD Received 1 Nov 2012; revised 14 Dec 2012; accepted 21 Dec 2012; published 7 Jan 2013

the SSII based on the SSII theory, and the calculated result can be further feedback to carry out the SSII cancellation. Since the SSII of each subcarrier will be calculated individually, the SSII cancellation is performed after the FFT. Then the OFDM data after the SSII cancellation are demodulated again, and the iterative process would get the more correct detected data.

Based on the SSII theory in Sec. 2, SSII is composed of the beating and intermixing terms, which are caused by the square-law photo-detection and the square-root-law amplitude modulation and chirp-induced phase modulation, respectively. Consequently, following the model of the whole optical transmission system, SSII could be estimated by iteratively replacing v_n by the detected data, $v_n^{(i-1)}$, where the superscript, i, denotes the number of iteration. The detail of the block of SSII calculation of Fig. 1 is shown in Fig. 2(a), and SSII calculation is composed of three parts, transmitted signal reconstruction, emulated SSII calculation, and calculated SSII modification. In the block of the transmitted signal reconstruction, the detected OFDM data $v_n^{(i-1)}$ is multiplied with the frequency response of optical transmitter, $H_T(n)$, the transmitted AC power envelop $X_1^{(i)}$ of the OFDM signal can be reconstructed, and then be sent to the block of emulated SSII calculation.

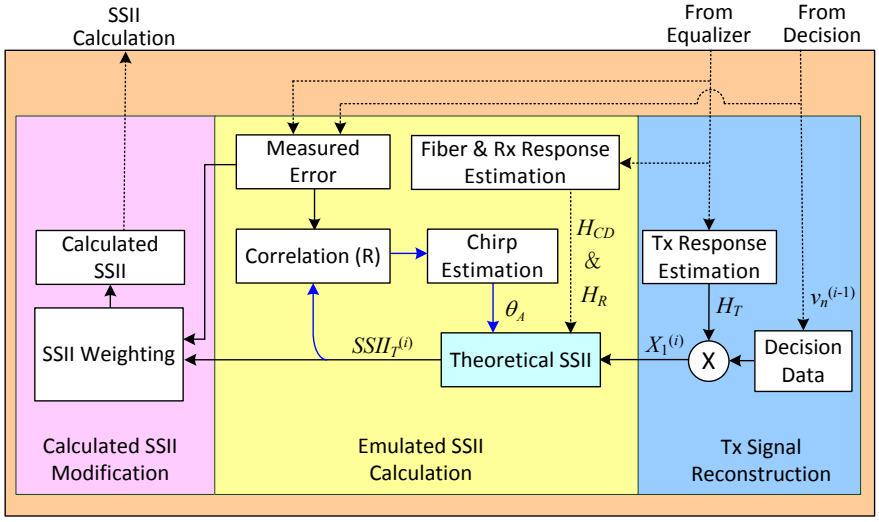

(a)

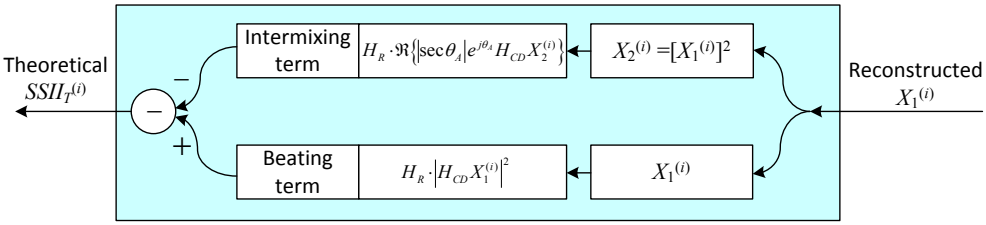

(b)

Fig. 2. The detail block diagrams of the (a) SSII calculation and (b) theoretical SSII.

In the block of emulated SSII calculation, the reconstructed transmitted power envelop $X_1^{(i)}$ of optical OFDM signal will be firstly sent to the block of theoretical SSII to get theoretical $SSII_T^{(i)}$ based on the SSII theory. The detail block diagram of theoretical SSII of Fig. 2(a) is shown in Fig. 2(b). The 2nd order term $X_2^{(i)}$ can be derived from the $X_1^{(i)}$. After applying the estimated responses including $H_{CD}(n)$ and $H_R(n)$, the beating and intermixing terms can be calculated and combined to rebuild the theoretical $SSII_T^{(i)}$. Besides, according to

#178232 - $15.00 USD Received 1 Nov 2012; revised 14 Dec 2012; accepted 21 Dec 2012; published 7 Jan 2013

Eq. (3), the chirp-related parameter, θ_A, is needed to calculate the intermixing terms. Therefore, in the block of emulated SSII calculation, maximizing the correlation coefficient R between the measured error and the theoretical $SSII_T^{(i)}$ is used to estimate the chirp-related parameter, θ_A. Notably, the correlation coefficient R could not be unity, because the actual error includes noise and higher-order nonlinear terms. Once the SSII dominates the error, R will approach unity. Moreover, the amplitude of the theoretical $SSII_T^{(i)}$ has to be corrected, since the required knowledge of x_n is composed of not only v_n but also a normalization factor, which is related to the difficultly measured optical modulation index (OMI). Consequently, in the block of calculated SSII modification, the theoretical $SSII_T^{(i)}$ will be modified by SSII weighting, which applies linear least squares fitting to minimize the sum of the squares of the deviations between the measured error and the theoretical $SSII_T^{(i)}$. Moreover, since $[X_1^{(i)}]^2$ and $|H_{CD}X_1^{(i)}|^2$ shown in Fig. 2(b) involves the discrete convolution in the frequency domain, the additional computational complexity of the proposed SSII cancellation technique mainly comes from calculating theoretical SSII. The convolution of two discrete spectra can be realized by multiplying their inverse Fourier transforms in the time domain followed by applying Fourier transform. Each transform and inverse transform requires $O((2N)\times\log_2(2N))$ operations, and the multiplication requires $O(2N)$ operations [14]. Thus, the extra computational complexity of $O((2N)\times\log_2(2N))$ is required for each iteration.

As for the response measurements of $H_T(n)$, $H_{CD}(n)$ and $H_R(n)$, the response of the optical receiver $H_R(n)$ is assumed flatten in the beginning. Then, through measuring the responses of optical back-to-back signals and optical fiber transmission by the training symbols, the responses of $H_T(n)$ and $H_{CD}(n)$ can be obtained. Then, the inaccuracy of the assumed $H_R(n)$ is compensated by SSII weighting in the block of calculated SSII modification. However, since the SSII power is generally much lower than the power of subcarriers, SSII-to-noise ratio would be low [7,12] and the presence of noise will degrade the accuracy of both chirp estimation and SSII weighting. Therefore, we need to increase the number of training symbols at the price of lower bandwidth efficiency. Nonetheless, since chirp estimation and SSII weighting are dependent on the operation conditions of the transmitter but almost irrelevant to the slowly-varying response of fiber channel, long training symbol can be just used in the beginning or used occasionally, and normal training symbol format can be used after the required parameters of SSII cancellation have been estimated.

4. Experimental set-up and results

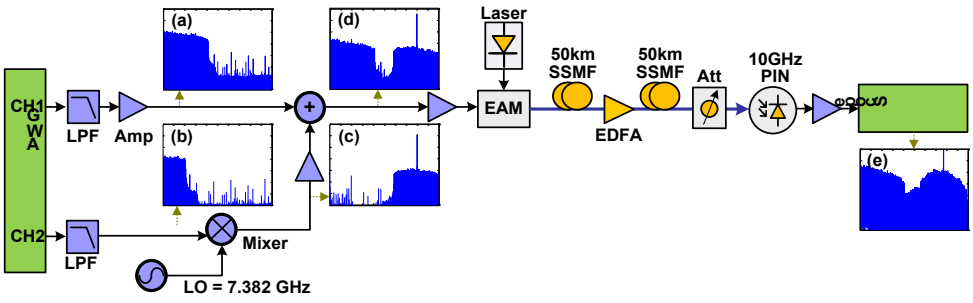

Fig. 3. Experimental setup with spectrum illustrations. (a) channel 1, (b) channel 2, (c) channel 2 after up-conversion, and (d) combination of channels 1 and 2.

In this work, the purpose is to verify the SSII cancellation technique, we just simply adopt two-band OFDM signal format without using bit-loading algorithm. The experimental setup

#178232 - $15.00 USD Received 1 Nov 2012; revised 14 Dec 2012; accepted 21 Dec 2012; published 7 Jan 2013

is similar with our previous work [7] and the differences are only the subcarrier allocations. A point-to-point transmission is adopted to emulate a long-reach OFDM-PON, since the loss of a remote node in PONs can be compensated by an optical amplifier. The baseband electrical OFDM signal is generated by an arbitrary waveform generator (AWG, Tektronix® AWG7122) using Matlab® programs. The signal processing of the OFDM transmitter consists of serial-to-parallel conversion, QAM symbol encoding, inverse fast Fourier transform (IFFT), cyclic prefix (CP) insertion, and DAC. The sampling rate and DAC resolution of the AWG are 12 GS/s and 8 bits, respectively. Other detailed parameters of generated OFDM signals include the FFT size of 512, the CP size of 8. The channel-1 OFDM signal is located in the 1st passband, and it consists of 23.4375-MSym/s 64-QAM and QPSK symbols, which are encoded at the 2nd-124th and 125th-164th subcarriers, respectively. Thus, the channel-1 signal contains 163 subcarriers with 3.82-GHz bandwidth, yielding a total data rate of 19.1718 Gbps. The channel-2 OFDM signal of the same symbol rate but with 32-QAM and QPSK formats are encoded at the 2nd-44th and 45th-76th subcarriers, and then it is up-converted to 7.382 GHz, which is equivalent to the frequency of the 315th subcarrier. Thus, the up-converted OFDM signal occupies the 239th-313rd and 317th-391st subcarriers located in the 2nd passband, and it contains 150 subcarriers with 3.5-GHz bandwidth. Notably, since the channel number of the AWG is only 2, this up-converted signal is used to emulate a 13.0781-Gbps signal which should be realized by independent I- and Q-channels in practical. Through a power coupler, both OFDM bands are then combined, and a total data rate of 32.25 Gbps is achieved. The insets (a)-(d) of Fig. 3 exhibit the electrical spectra of the channel-1 signal, the channel-2 signal, and the up-converted channel-2 signal, and the combined 2-band signal, respectively. The combined OFDM signal is then sent to the EAM to generate an optical DSB OFDM signal. After 100 km of SSMF transmission and direct-detection, the received electrical signal is captured by a digital oscilloscope (Tektronix® DPO 71254) with a 50-GS/s sampling rate and a 3-dB bandwidth of 12.5 GHz, and the spectrum is shown in the inset (e) of Fig. 3. Due to the limited buffer size of oscilloscope, 1000 OFDM symbols with 1.707 Megabits are captured. An off-line Matlab® DSP program is used to demodulate the OFDM signals and the demodulation process includes synchronization, FFT, one-tap equalization, and QAM symbol decoding. Lastly, BERs are counted by bit-by-bit comparison between the detected data and transmitted data. In order to accurately estimate the required parameters of SSII cancellation, enough training symbols must be adopted in the beginning, and 50 training symbols are adopted in this work. Thus, SSII can be calculated and cancelled based on SSII cancellation technique as shown Fig. 1. Moreover, although the iterative process is expected to reduce the influence of the decision errors of $v_n^{(i-1)}$ on estimating SSII, our experimental results do not show further improvement provided by iteration, so that the SSII cancellation technique is applied without iteration throughout this work. The reason would be the SSII is contributed by a lot of subcarriers, and a few decision errors may not affect the estimation much around the BER of interest [12]. As a result, the computational complexity can be lowered by omitting the iterative process in this case. However, significant decision errors may be contributed by higher SSII due to longer SSMF (>100 km) and/or more frequency chirp. In this condition, the iterative process could be adopted to decrease the decision errors and improve the accuracy of SSII estimation [12]. Figure 4 shows the electrical spectra of the OFDM signal composed of two bands after 100-km transmission shown by blue curve and the calculated SSII shown by red curve. Since the subcarriers at 5.6~8.4 GHz are overlapped with the most of SSII, they suffer from severer SNR penalties.

Figure 5(a) shows the measured SNR of each OFDM subcarrier. The SNR after 100-km SSMF transmission without SSII cancellation is shown by red curve in Fig. 5(a), and the SNR shown by black curve is measured by transmitting band-1 and band-2 OFDM signals individually. Theoretically, if only the band-2 signal is transmitted, the signal will not suffer the SSII induced by itself, or equivalently, all the SSII is out-of-band. In addition, for the case of band-1 only, the influence of the SSII can be ignored, as shown in Fig. 4. Thus, the SNR

#178232 - $15.00 USD Received 1 Nov 2012; revised 14 Dec 2012; accepted 21 Dec 2012; published 7 Jan 2013

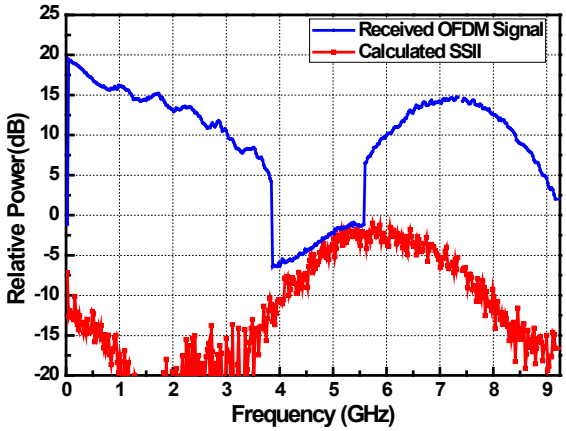

Fig. 4. Electrical spectra of the OFDM signal composed of two bands after 100-km transmission and the calculated SSII.

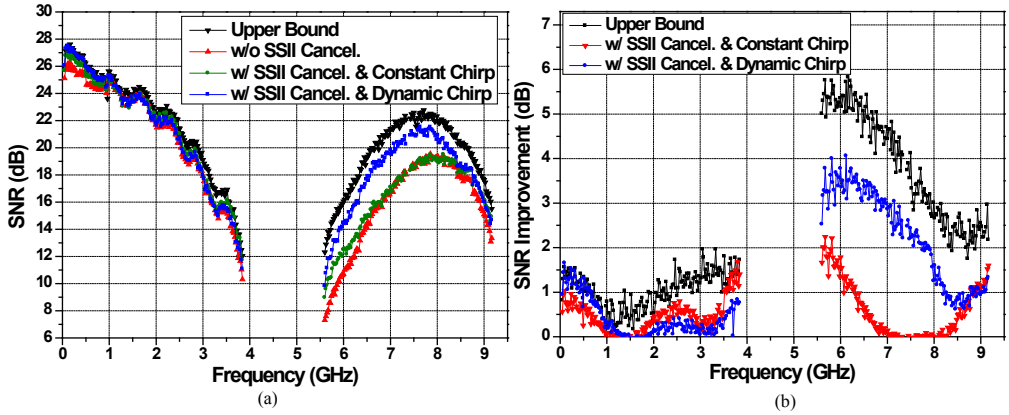

Fig. 5. (a) SNR of each subcarrier of optical back-to-back, one-band OFDM after 100-km SSMF, two-band OFDM after 100-km SSMF without SSII cancellation, and two-band OFDM after 100-km SSMF with SSII cancellation via considering the constant chirp and the dynamic chirp. (b) SNR improvement by SSII cancellation of three cases corresponding to those in (a).

difference between red and black curves can be regarded as the upper bound of SSII cancellation. After introducing the SSII cancellation technique with only considering the constant chirp parameter α_0 of EAM, which is about 0.53 at the bias voltage of –1 V measured by the method in [15], as shown by green curve in Fig. 5(a), we can find that the SSII cancellation is not obvious. After considering the dynamic chirp parameter including α_0 and α_1, as shown by blue curve in Fig. 5(a), the black and blue curves are almost overlapped and the SSII can be almost canceled. Thus, from both the SSII theory shown in Sec. 2 and the experimental results shown in Fig. 5(a), the dynamic chirp must be taken into consideration to improve the performance of SSII cancellation. Figure 5(b) shows the SNR improvement by SSII cancellation of three cases corresponding to those in Fig. 5(a).

To evaluate the performance of the SSII cancellation technique, the average amount of SSII elimination is to be defined and calculated. For the n^{th} subcarrier, if the received signal power, the noise power and the SSII power without the SSII cancellation are denoted as $P_S(n)$, $P_N(n)$ and $P_{SSII,W}(n)$, respectively, the corresponding SNR could be written as $\Gamma_W(n) = P_S(n)/[P_{SSII,W}(n) + P_N(n)]$. Since we assume no SSII for the case of the upper bound, its SNR will be $\Gamma_U(n) = P_S(n)/P_N(n)$. Furthermore, the power of residual SSII after SSII cancellation is

#178232 - $15.00 USD Received 1 Nov 2012; revised 14 Dec 2012; accepted 21 Dec 2012; published 7 Jan 2013

set as $P_{SSII,C}(n)$ or $P_{SSII,D}(n)$, where the subscript C or D indicates the cancellation based on the constant chirp model or the dynamic chirp model. Hence, the SNR after the SSII cancellation will be $\Gamma_C(n) = P_S(n)/[P_{SSII,C}(n) + P_N(n)]$ or $\Gamma_D(n) = P_S(n)/[P_{SSII,D}(n) + P_N(n)]$. Consequently, the power of SSII could be estimated by the SNRs and the signal power,

$$P_{SSII,\zeta}(n) = \frac{P_S(n)}{\Gamma_\zeta(n)} - \frac{P_S(n)}{\Gamma_U(n)}, \tag{4}$$

where the subscript $\zeta \in \{W, C, D\}$. Moreover, the amount of SSII elimination could be obtained by $\Delta P_{SSII,C}(n) = P_{SSII,W}(n) - P_{SSII,C}(n)$ or $\Delta P_{SSII,D}(n) = P_{SSII,W}(n) - P_{SSII,D}(n)$. Then the average amount of SSII elimination in percentage can be written as

$$\overline{\Delta P}_{SSII,\zeta} = \frac{\sum_{n=1}^{N} \Delta P_{SSII,\zeta}}{\sum_{n=1}^{N} P_{SSII,W}}. \tag{5}$$

If the constant chirp is considered, the proposed SSII cancellation technique can only achieve 23.6% SSII elimination. However, employing the new dynamic chirp model, 74.4% SSII elimination can be achieved which demonstrates a considerable effectiveness of the new model.

Based on the dynamic chirp model, Fig. 6 shows the measured SNR improvement with different numbers of training symbols. With only 10 training symbols, the estimation of SSII weighting is inaccurate and the SNR improvement is much less than those with more training symbols. As the number of training symbols increasing, the SNR improvement will be improved. However, 50 training symbols are sufficient to accurately estimate SSII weighting, and further increment of training symbols does not improve the signal performance much, as shown in Fig. 6. Thus, in order to optimize the performance of SSII cancellation and also maintain the bandwidth efficiency, 50 training symbols are adopted in this work. Moreover, according to Eq. (5), 66.8%, 73.5%, 75.0% and 75.1% SSII eliminations are achieved by using 10, 30, 70, and 90 training symbols, respectively.

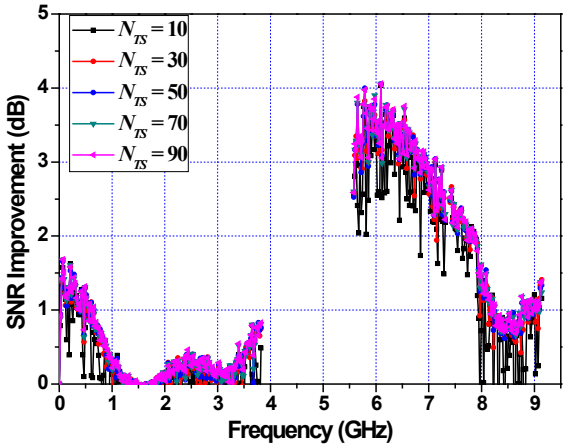

Fig. 6. SNR improvement with different numbers of training symbol, N_{TS}.

Furthermore, the BER performances of the EAM-based OFDM signal with five cases are plotted in Fig. 7(a). In Fig. 7(a), the cases (i) and (ii) shown by the black and green solid circles indicate the cases of optical back-to-back (O B-t-B) and 100-km SSMF without SSII cancellation, respectively, while the cases (iii) and (iv) shown by the red and blue solid circles

#178232 - $15.00 USD Received 1 Nov 2012; revised 14 Dec 2012; accepted 21 Dec 2012; published 7 Jan 2013

indicate the cases of using the SSII cancellation technique with considering the constant and dynamic chirp parameters of EAM, respectively. The BER of ~3.8×10^{-3} (the FEC limit) of cases (ii), (iii) and (iv) can be obtained at the received powers of –8.4 dBm, –10.2 dBm, and –11.2 dBm. Accordingly, after using the SSII cancellation technique with considering the constant and dynamic chirp parameters, the receiver sensitivities are improved by 1.8 dB and 2.8 dB, respectively. In addition, assuming the full knowledge of the transmitted data is known and used for the SSII estimation and cancellation, the BER performance with such ideal SSII cancellation is also plotted as the case (v) in Fig. 7(a). Compared with the ideal SSII cancellation, the proposed SSII cancellation without iteration almost shows identical performance, and therefore, the iteration process can be dropped in this experiment. Moreover, corresponding to the cases (ii) and (iv) at the received power of –6 dBm, the constellations of the 32-QAM and QPSK in the 2nd passband before and after SSII cancellation are shown in Fig. 7(b) for comparison.

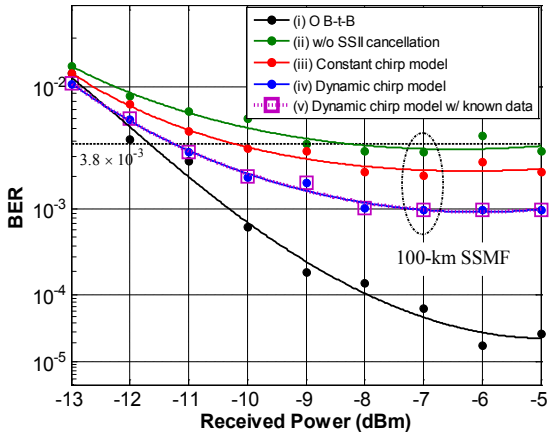

(a)

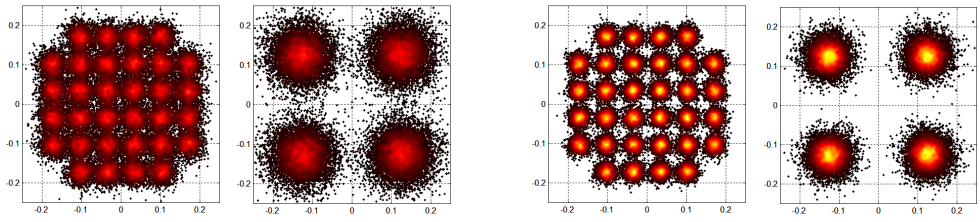

Before SSII Cancellation

After SSII Cancellation

(b)

Fig. 7. (a) BER and (b) constellations of OFDM signals before and after SSII cancellation.

5. Conclusion

In this paper, a novel SSII cancellation technique is proposed and experimentally demonstrated in an EAM-based IMDD OFDM transmission system for the first time. Incorporating the dynamic chirp model into the SSII cancellation technique shows that the SSII elimination can be improved from 23.6% to 74.4%, compared with the constant chirp model, and 2.8-dB sensitivity improvement can be achieved in a 32.25-Gbps OFDM system over 100-km uncompensated SSMF. Moreover, compared with the back-to-back case, the 32.25-Gbps EAM-based OFDM signal shows only 0.5-dB penalty after 100-km uncompensated SSMF. Thus, combining the novel SSII cancellation technique proposed in this work and the optical multi-band OFDM with adaptive modulation in our previous work

#178232 - $15.00 USD Received 1 Nov 2012; revised 14 Dec 2012; accepted 21 Dec 2012; published 7 Jan 2013

[7], the IMDD OFDM-PON will not be limited by the SSII and power fading, and become a feasible and economical solution for LR-PONs.

#178232 - $15.00 USD Received 1 Nov 2012; revised 14 Dec 2012; accepted 21 Dec 2012; published 7 Jan 2013